Advances in Water Resources xxx (2011) xxx–xxx

Contents lists available at ScienceDirect

Advances in Water Resources

journal homepage: www.elsevier.com/locate/advwatres

The effect of heterogeneity on the character of density-driven natural convection of CO_2 overlying a brine layer

R. Farajzadeh [a,*], P. Ranganathan [b], P.L.J. Zitha [b], J. Bruining [b]

[a] Shell International Exploration and Production, 2288 GS Rijswijk, The Netherlands
[b] Delft University of Technology, Department of Geotechnology, Stevinweg 1, 2628 CN Delft, The Netherlands

ARTICLE INFO

Article history:
Received 25 August 2010
Received in revised form 25 December 2010
Accepted 26 December 2010
Available online xxxx

Keywords:
Density-driven natural convection
CO_2
Porous media
Mass transfer
Heterogeneity

ABSTRACT

The efficiency of mixing in density-driven natural-convection is largely governed by the aquifer permeability, which is heterogeneous in practice. The character (fingering, stable mixing or channeling) of flow-driven mixing processes depends primarily on the permeability heterogeneity character of the aquifer, i.e., on its degree of permeability variance (Dykstra–Parsons coefficient) and the correlation length. Here we follow the ideas of Waggoner et al. (1992) [13] to identify different flow regimes of a density-driven natural convection flow by numerical simulation. Heterogeneous fields are generated with the spectral method of Shinozuka and Jan (1972) [13], because the method allows the use of power-law variograms. In this paper, we extended the classification of Waggoner et al. (1992) [13] for the natural convection phenomenon, which can be used as a tool in selecting optimal fields with maximum transfer rates of CO_2 into water. We observe from our simulations that the rate of mass transfer of CO_2 into water is higher for heterogeneous media.

1. Introduction

Efficient storage of carbon dioxide (CO_2) in aquifers requires dissolution in the aqueous phase. Indeed the volume available for gaseous CO_2 is less than for dissolved CO_2. The inverse partial molar volume (virtual density) of dissolved CO_2 is around 1300 kg/m^3 [1] leading to more efficient storage than CO_2 remaining in the supercritical state (<600 kg/m^3) at relevant storage temperatures. Moreover, dissolution of CO_2 in water decreases the risk of CO_2 leakage. The mass transfer between CO_2 and underlying brine in aquifers causes a local density increase [1], which induces convection currents increasing the rate of CO_2 dissolution [2–4]. This system is gravitationally unstable and leads to unstable mixing enhancement in the aquifer [5–8].

The effect of natural convection increases with increasing Rayleigh number, which, for a constant-pressure CO_2-injection scheme, mainly depends on the permeability. This means that the efficiency of the mixing (caused by natural convection) is largely governed by the aquifer permeability [8,9], which is subject to spatial and directional variations in practice. Previous studies on this subject are mostly concerned with homogeneous porous media and despite attention of a few papers [9–12] the effect of heterogeneity on the CO_2 mass transfer in aquifers is not fully understood.

Fingering is the dominant flow pattern in density driven natural convection flows in homogeneous media [5,7,8]. However, CO_2 transport in heterogeneous media will be different than in homogeneous media because in the former case the permeability variations results in time-dependent velocity fluctuations, which in turn influence the mixing process. Waggoner et al. [13] investigated flow regimes for miscible displacement through permeable media under vertical-equilibrium (VE) conditions. Depending on the degree of heterogeneity (represented by the Dykstra–Parsons coefficient, V_{DP}) and continuity of the system (correlation length λ_R), they distinguished flow regimes that are dominated by fingering, dispersion, and channeling. The mixing zone displays different characteristics in these respective regimes. Mixing grows with the square root of time if dispersion dominates, whereas the growth is linear for displacements dominated by channeling and fingering. The principal difference between fingering and channeling is that a fingering displacement becomes dispersive when mobility ratio is less than one whereas a channeling displacement keeps the same character, albeit to a lesser degree. The work of Waggoner et al. [13] is extended by Sorbie et al. [14] for more general cases and by Chang et al. [15], who include density variations. Based on these studies viscous fingering is a dominant pattern in laboratory scale (or in quasi-homogeneous fields), but does not occur in the field where V_{DP} typically varies between 0.6 and 0.8 (in some exceptional cases V_{DP} can have values as large as 0.9).

* Corresponding author.
E-mail address: r.farajzadeh@tudelft.nl (R. Farajzadeh).

0309-1708/$ - see front matter © 2010 Elsevier Ltd. All rights reserved.
doi:10.1016/j.advwatres.2010.12.012

Nomenclature

A	aspect ratio, H/L [–]
c	dimensionless concentration [–]
c'	concentration [mole/m^3]
D	diffusion coefficient [m^2/s]
g	acceleration due to gravity [m/s^2]
G	gravity number [–]
H	height of the porous medium [m]
k	permeability of the porous medium [m^2]
L	length of the porous medium [m]
M	mobility ratio [–]
p	pressure [Pa]
Ra	Rayleigh number [–]
s	distance between points
S_i	iD spectral density function (i = 1,2,3)
t	time [s]
u	dimensionless velocity [–]
U	velocity [m/s]
V_{DP}	Dykstra–Parsons coefficient
x_i	x, y and z position for i = 1, 2, 3
X	dimensionless distance in X coordinate
Z	dimensionless distance in Z coordinate

Greek symbols

β_c	volumetric expansion factor [m^3/mole]
δ	amplitude [–]
φ	porosity of the porous medium [–]
Φ	random phase angle
γ	semivariogram
λ_R	dimension less correlation length [–]
μ	viscosity of the fluid [kg/m s]
ψ	Stream function [m^3/m s]
ρ	density of the fluid [kg/m^3]
σ	standard deviation, square root of variance [–]
τ	dimensionless time [–]
ω	weighting function

Subscripts

0	value of the quantity at the boundary
1	x direction or 1D
2	y direction or 2D
3	z direction or 3D
i	reference value of the quantity
x	quantity in x-direction
z	quantity in z-direction

The aim of this paper is to investigate the effect of heterogeneity on the character of natural-convection flow of CO_2 in aquifers and on the dissolution rate of CO_2 in brine. The permeability fields were generated using the Dykstra–Parson coefficient, V_{DP} (measure of extent of heterogeneity) and spatial correlation length, λ_R (indicator of permeability-field correlation) as characterizing parameters. We follow the approach proposed by Waggoner et al. [13] to characterize flow regimes (fingering, dispersive, and channeling) corresponding to density-driven natural-convection flow of CO_2. The structure of the paper is as follows: first we describe the formulation of the physical model and introduce the ensuing equations. Then we briefly explain the method used to generate the permeability fields. Next we demonstrate the simulation results, and discuss their implications. We end the paper with some concluding remarks.

2. Physical model

2.1. Formulation

We consider a fluid saturated porous medium with a height H and length L, as depicted in Fig. 1. The constant porosity of the porous medium is φ and its permeability varies spatially, i.e., $k = k(x,z)$. Initially the fluid is at rest and there is no CO_2 dissolved in the fluid. We assume no flow boundary at the sides and the bottom of the porous medium. CO_2 is continuously supplied from the top, i.e., the CO_2 concentration at the top is kept constant. We assume that the CO_2–liquid interface is sharp and fixed. We disregard the presence of a capillary transition zone between the gas and the liquid phase. Hence we only model the liquid phase and the presence of the gas phase at the top is represented by a boundary condition for the liquid phase. The motion of fluid is described by Darcy's law driven by a density gradient. Darcy's law is combined with the mass conservation laws for the two components (CO_2 and water or CO_2 and oil) to describe the diffusion and natural-convection processes in the porous medium. We only expect a laminar regime since the Rayleigh number is low. We use the Boussinesq approximation which considers density variations only when they contribute directly to the fluid motion.

2.2. Governing equations

For the 2D porous medium depicted in Fig. 1, the governing equations can be written as

(a) *Continuity equation*

$$\varphi\frac{\partial\rho}{\partial t}+\frac{\partial(\rho U_X)}{\partial X}+\frac{\partial(\rho U_Z)}{\partial Z}=0. \tag{1}$$

(b) *Darcy's law*

$$U_X=-\frac{k_m f(X,Z)}{\mu}\frac{\partial p}{\partial X}, \tag{2}$$

$$U_Z=-\frac{k_m f(X,Z)}{\mu}\left(\frac{\partial p}{\partial Z}-\rho g\right). \tag{3}$$

In these equations $f(X,Z)$ describes the variations of permeability with respect to average permeability, k_m. In other words, $k(X,Z) = k_m f(X,Z)$.

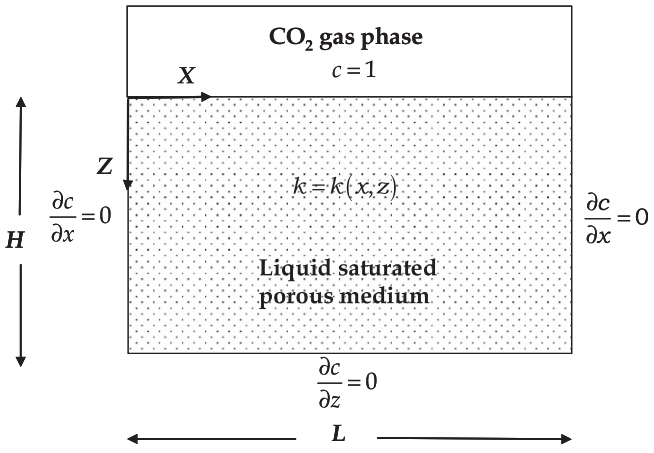

Fig. 1. Schematic of the system and coordinates.

Please cite this article in press as: Farajzadeh R et al. The effect of heterogeneity on the character of density-driven natural convection of CO_2 overlying a brine layer. Adv Water Resour (2011), doi:10.1016/j.advwatres.2010.12.012

(c) *Concentration*

$$\frac{\varphi\partial c'}{\partial t}+U_X\frac{\partial c'}{\partial X}+U_Z\frac{\partial c'}{\partial Z}=\varphi D\left(\frac{\partial^2 c'}{\partial X^2}+\frac{\partial^2 c'}{\partial Z^2}\right). \quad (4)$$

In our case the relevant Peclet number will be less than one, meaning that the mixing will be mainly determined by molecular diffusion [49] and therefore D is taken to be the molecular diffusion coefficient in our model.

CO_2 dissolution at the top increases the fluid density. The dissolved concentration of CO_2 is small meaning that the density variations can be represented by the following equation:

$$\rho=\rho_0\left(1+\beta_c\left(c'-c'_0\right)\right) \quad (5)$$

from which we obtain

$$\frac{\partial\rho}{\partial X}=\rho_0\beta_c\frac{\partial c'}{\partial X}. \quad (6)$$

In Eqs. (1)–(4) we have four unknowns (U_x, U_z, p, and c'). It is possible to eliminate the pressure by differentiating Eq. (2) with respect to Z and Eq. (3) with respect to X and subtract the result. This leads to

$$\frac{\partial(U_Z/k(X,Z))}{\partial X}-\frac{\partial(U_X/k(X,Z))}{\partial Z}=\frac{1}{\mu}\left[-\frac{\partial}{\partial X}\left[\left(\frac{\partial p}{\partial Z}-\rho g\right)\right]+\frac{\partial}{\partial Z}\left[\frac{\partial p}{\partial X}\right]\right]=\frac{1}{\mu}\frac{\partial\rho}{\partial X}g=\frac{g\rho_0\beta_c}{\mu}\frac{\partial c'}{\partial X}. \quad (7)$$

Therefore, the equations to be solved are Eqs. (1), (4) and (7) to obtain U_x, U_z, and c'.

2.3. Dimensionless form of the equations

We take H as characteristic length and define the following dimensionless variables

$$x=\frac{X}{H},\quad z=\frac{Z}{H},\quad u_x=\frac{H}{\varphi D}U_X,\quad u_z=\frac{H}{\varphi D}U_Z,$$
$$\tau=\frac{D}{H^2}t,\quad c=\frac{c'-c'_i}{c'_0-c'_i}$$

$$u_x=-\frac{\partial\psi}{\partial z},\quad u_z=\frac{\partial\psi}{\partial x},\quad Ra=\frac{k_m\rho_0\beta_c gH\Delta c'}{\varphi D\mu}=\frac{\Delta\rho g k_m H}{\varphi D\mu} \quad (8)$$

Thus, after applying the Boussinesq approximation the dimensionless form of the Eqs. (7) and (4) can be respectively written as

$$\frac{\partial}{\partial x}\left(\frac{1}{f(x,z)}\frac{\partial\psi}{\partial x}\right)+\frac{\partial}{\partial z}\left(\frac{1}{f(x,z)}\frac{\partial\psi}{\partial z}\right)=Ra\frac{\partial c}{\partial x} \quad (9)$$

and,

$$\frac{\partial c}{\partial\tau}-\frac{\partial\psi}{\partial z}\frac{\partial c}{\partial x}+\frac{\partial\psi}{\partial x}\frac{\partial c}{\partial z}=\frac{\partial^2 c}{\partial x^2}+\frac{\partial^2 c}{\partial z^2}. \quad (10)$$

2.4. Boundary and initial conditions

The initial condition of the problem is

$$\psi=0,\quad c=0\quad \text{at } \tau=0. \quad (11)$$

The boundary conditions of the problem are

$$\psi=0,\quad \frac{\partial c}{\partial z}=0\quad \text{at } x=0,\quad \psi=0,\quad c=1\quad \text{at } z=0,$$
$$\psi=0,\quad \frac{\partial c}{\partial x}=0\quad \text{at } z=1,\quad \psi=0,\quad \frac{\partial c}{\partial x}=0\quad \text{at } x=A. \quad (12)$$

Note that the boundaries of the domain limit the mixing of CO_2, i.e., if the width of the domain decreases the transfer rate also decreases [8].

2.5. Solution procedure

A modified version of the numerical method explained by Güçeri and Farouk [16], i.e., the finite volume approach, was applied to solve the system of Eqs. (9) and (10). A fully implicit method was used to obtain the transient values in Eq. (10). For each time step, we first compute the stream function from Eq. (9) and then we obtain the concentration profile by solving Eq. (10). The calculation procedure for each time step was repeated until the following criteria were satisfied

$$\left|\frac{c_{i,j}^{\tau+\Delta\tau}-c_{i,j}^{\tau}}{c_{i,j}^{\tau+\Delta\tau}}\right|_{\max}\leqslant\varepsilon\quad\text{and}\quad\left|\frac{\psi_{i,j}^{\tau+\Delta\tau}-\psi_{i,j}^{\tau}}{\psi_{i,j}^{\tau+\Delta\tau}}\right|_{\max}\leqslant\varepsilon, \quad (13)$$

where ε was set to 10^{-5} in the numerical computations reported in this paper and the time step was chosen to be 10^{-5} ($V_{DP}<0.8$) and 10^{-6} ($V_{DP}=0.8$) to obtain accurate results.

To observe the non-linear behavior, i.e., the fingering behavior it was necessary to disturb the interface. Therefore in the numerical simulations, we start with a wavy perturbation on the top interface, i.e.,

$$c(x,z=0,t=0)=1+A_0\sin(2\pi x/\lambda), \quad (14)$$

where $A_0=0.01$ and $\lambda=1/12$. In reality fluctuations are caused by thermodynamic fluctuations [17,18] and pore-level perturbations. We ignore instabilities on the pore level (see, however, e.g. Refs. [19,20]).

2.6. Interpretation

2.6.1. Effective dispersion coefficient

It is our aim to derive the character of the displacement process, i.e., whether it is mainly diffusive or convective. To interpret the result we adapt the method explained in detail in Ref. [21]. First we average the concentration profile in the x-direction and divide by the concentration at the gas–liquid boundary to obtain $\partial\hat{c}(z,t)$. This concentration can be considered as a complementary cumulative distribution function and its derivative towards z as a probability density function. For convenience we add the symmetric part to the probability density function $p(z,t)$ such that

$$p(z,t)=-\frac{1}{2}\left(\frac{\partial\hat{c}(|z|,t)}{\partial z}\right). \quad (15)$$

The variance σ_c^2 of the concentration profile is given by,

$$\sigma_c^2=2\int_0^\infty z^2p(z,t)dz,=2\int_0^\infty z\hat{c}(|z|,t)dz, \quad (16)$$

where we used integration by parts. If the process were purely diffusive we would obtain that $\hat{c}(z,t)=\mathrm{erfc}(z/2\sqrt{(Dt)})$, where D is the diffusion coefficient. In this case $\sigma_c^2=2Dt$ and hence we will interpret $D(t)=1/2d\sigma_c^2/dt$ as a diffusion coefficient. When the diffusion coefficient is independent of time the process is considered diffusive; if it is more proportional to time it is considered convective. If, in the latter case, the concentration profile develops along high permeability paths we will call it channeling, if it develops arbitrarily we call it fingering.

2.6.2. Other measures of heterogeneity

Coefficient of variation, C_V: The coefficient of variation is a measure of sample variation or dispersion and expresses the standard deviation, σ, as a fraction of sample mean, k_m [22]. It is defined as:

Please cite this article in press as: Farajzadeh R et al. The effect of heterogeneity on the character of density-driven natural convection of CO_2 overlying a brine layer. Adv Water Resour (2011), doi:10.1016/j.advwatres.2010.12.012

$C_V = \sigma/\bar{k}$. Samples with $C_V < 0.5$ are considered homogeneous and with $C_V > 1$ are assumed very heterogeneous [22].

Koval factor, H_K: The Koval heterogeneity factor [23] is typically used to account for unstable behavior of miscible displacement in heterogeneous porous media. The relation between V_{DP} and H_K is:

$$\log_{10}(H_K) = V_{DP}/(1 - V_{DP})^{0.2}. \quad (17)$$

Heterogeneity index, I_H: Gelhar–Axness coefficient or heterogeneity index [24] combines the degree of heterogeneity with the correlation length as

$$I_H = \sigma^2_{\ln k}\lambda_R, \quad (18)$$

where $\sigma^2_{\ln k}$ is the variance of log permeability fields and λ_R is the dimensionless correlation ($\lambda_R = \lambda/L$, where L is the system length).

Our aim is to find out whether there is a relation between the mass of dissolved CO_2 in water and the heterogeneity of the porous medium represented by one of the measures of heterogeneity.

3. Generation of stochastic random fields

Random field generators are widely used as a tool to model heterogeneities in porous media [25] for applications in hydrocarbon recovery and groundwater flow. The generated field can be used as model (permeability) fields for research work [13]. Prediction methods [26] for many realizations of such fields can quantify the uncertainty of expected product recoveries.

A number of methods have been conventionally employed to generate random fields [27–30]. First, we note that these conventional methods generate correlated random fields from a sum of terms and hence generate multi-Gaussian fields. Most earth-science phenomena are not multivariate Gaussian but can be transformed such that the resulting variable is approximately Gaussian for example the logarithm of the permeability [31]. This paper uses the spectral (Fourier) methods [32,33] to generate fields with exponential variograms [30], which only involves correlation over a single length scale. We leave an analysis using a permeability field that involves many length scales [30,34,50]; fractal fields [35]; wavelets [36,37]; Markov processes and non-Gaussian methods using Copula-based methods [38] for future work.

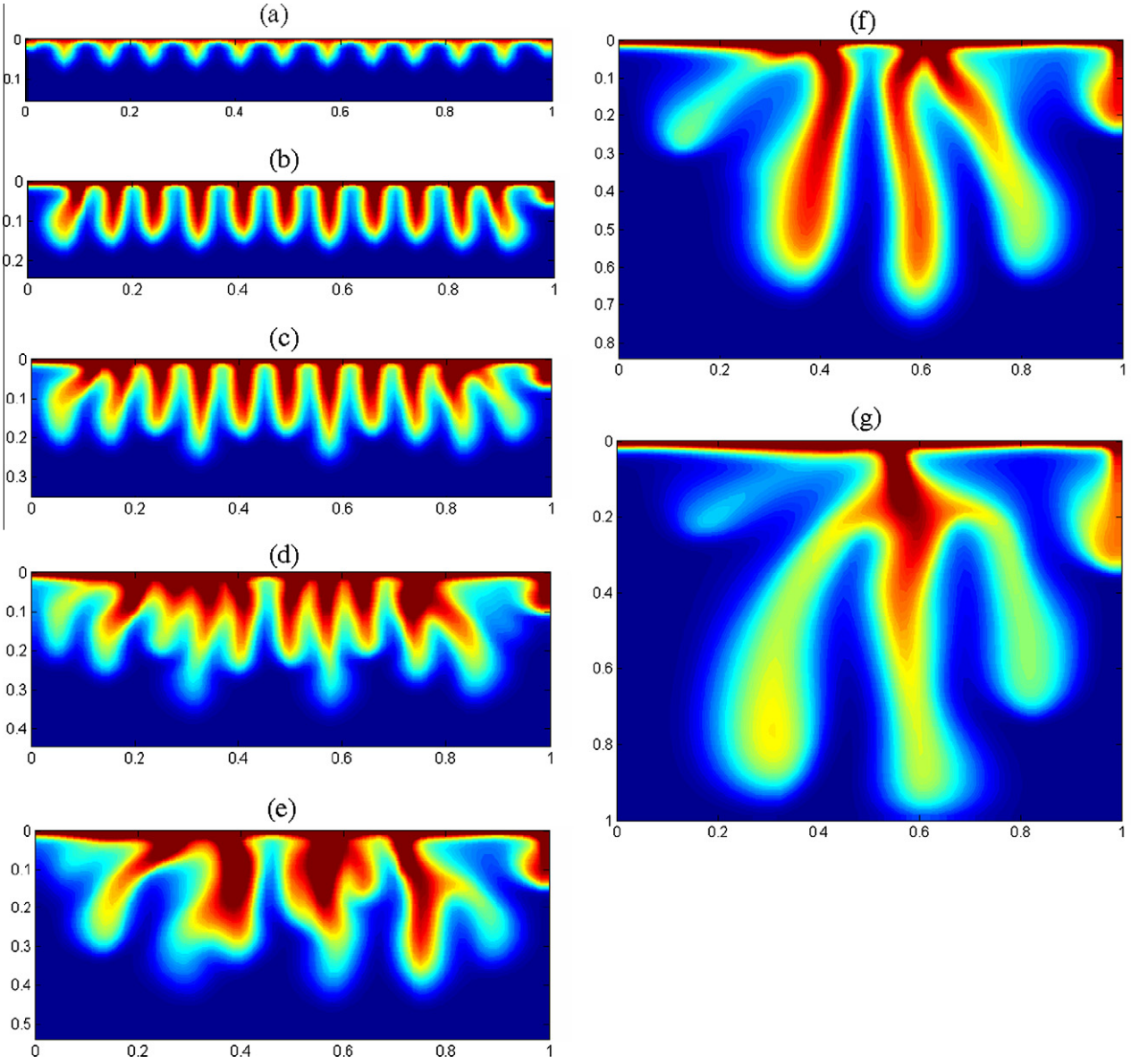

Fig. 2. Concentration profiles of the base case (homogeneous medium and $Ra = 5000$) at τ = (a) 0.0001, (b) 0.0003, (c) 0.0005, (d) 0.00075, (e) 0.001, (f) 0.0015 and (g) 0.002.

Please cite this article in press as: Farajzadeh R et al. The effect of heterogeneity on the character of density-driven natural convection of CO_2 overlying a brine layer. Adv Water Resour (2011), doi:10.1016/j.advwatres.2010.12.012

We use the following equation of a random field value for a two-dimensional field:

$$f(x_1,x_2)=\sqrt{2}\sum_{k=-N/2}^{N/2-1}\sum_{l=-N/2}^{N/2-1}(S_2(\omega_{kl})w(\omega_{1k},\omega_{2l}))^{\frac{1}{2}} \times \cos(\omega_{1k}x_1+\omega_{2l}x_2+\phi_{kl}). \quad (19)$$

The proof that Eq. (19) gives a field with the correct expected statistical properties is reproduced in Ref. [30]. In the equation, the indices 1 and 2 denote the x and z-direction. Application of Eq. (19) requires further information on the phase angle ω_{kl}, the spectral density function $S_2(\omega_{kl})$, the distribution of summation points and the weighting function $w(\omega_{1k},\omega_{2l})$. To avoid the occurrence of spurious symmetry patterns we added a small random frequency $\delta\omega$ to ω_{ik}, ω_{2l}, i.e., $\delta\omega = 0.05\pi/((N-1)b)(U(0,1)-1/2)$, where $U(0,1)$ denotes a uniformly distributed random variable with average zero and standard deviation one. The random phase angle ϕ_{kl} is distributed uniformly between 0 and 2π. In the spectral density function, denoted by $S_2(\omega_{kl})$, we use the abbreviation $\omega_{kl}=\sqrt{(\omega_{1k}^2+\omega_{1l}^2)}$ and the subscript 2 to denote 2D. The spectral density function corresponding to the exponential variogram $\gamma(h)=s^2(1-\exp(-h/\lambda))$ reads:

$$S_2(\omega)=\frac{s^2}{2\pi}\frac{1/\lambda}{(\omega^2+1/\lambda^2)^{3/2}}. \quad (20)$$

Eq. (19) represents a Fourier transform. Consequently, we use frequencies ω_{1k}; ω_{2l} in the range $[-\pi/b,\pi/b)$ where b is the distance between points. Also Nb is the system length and $\Delta\omega = 2\pi/(bN)$. We employ the full autocorrelation structure of the field only if the integral of the spectral density function over the thus-defined frequency space approaches σ^2. In other words, it is only useful to generate a field with a certain autocorrelation structure if the points in space are distributed sufficiently densely such that they indeed contain the information on the complete spectral density function

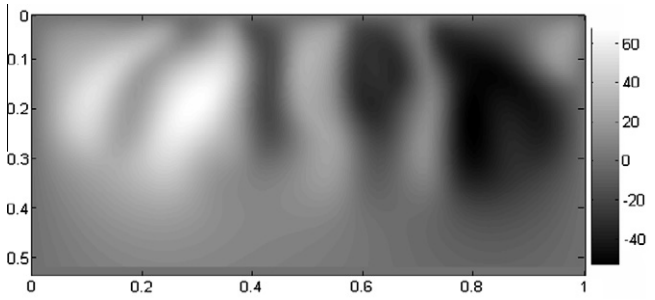

Fig. 3. Stream-function profile for $Ra = 5000$ at $\tau = 0.001$ corresponding to concentration profile in Fig. 2e.

Table 1
Labels of the permeability fields characterized by V_{DP} and λ_R.

Case ID	V_{DP}	λ_R	Case ID	V_{DP}	λ_R	Case ID	V_{DP}	λ_R	Case ID	V_{DP}	λ_R
P1P01	0.1	0.01	P3P01	0.3	0.01	P5P01	0.5	0.01	P8P01	0.8	0.01
P1P1	0.1	0.1	P3P1	0.3	0.1	P5P1	0.5	0.1	P8P1	0.8	0.1
P1P5	0.1	0.5	P3P5	0.3	0.5	P5P5	0.5	0.5	P8P5	0.8	0.5
P11	0.1	1	P31	0.3	1	P51	0.5	1	P81	0.8	1
P13	0.1	3	P33	0.3	3	P53	0.5	3	P83	0.8	3

Table 2
Output values of the stochastic model for input: $Ra = 5000$, $V_{DP} = 0.8$ ($\sigma_{\ln Ra} = 1.27$), and $\lambda_R = 1$.

Realization number	$\sigma_{\ln}Ra$	Output V_{DP}	Arithmetic average	Harmonic average	Heterogeneity index (I_H)	Koval factor	Coefficient of variation
1	0.97	0.62	1417.7	562.8	5.70	0.90	1.23
2	1.05	0.65	5269.8	1795.7	6.36	1.23	1.39
3	0.87	0.58	4244.3	2020.6	4.89	0.56	1.05
4	0.83	0.56	12929.0	6507.7	4.63	0.48	0.99
5	0.69	0.50	3582.4	2213.5	3.77	0.23	0.77
6	0.97	0.62	3657.2	1511.5	5.67	0.88	1.19
7	1.08	0.66	98335.0	33054.1	6.58	1.35	1.40
8	0.80	0.55	21823.4	11628.1	4.42	0.41	0.94
9	0.76	0.53	539.2	303.5	4.17	0.33	0.88
10	0.87	0.58	5959.5	2884.4	4.93	0.58	1.03

Table 3
Output values of the stochastic model for input: $Ra = 5000$ for two V_{DP} values.

Input V_{DP}	Input λ_R	$\sigma_{\ln}(Ra)$	Output V_{DP}	Arithmetic average	Harmonic average	Heterogeneity index (I_H)	Koval factor	Coefficient of variation
0.50	0.01	0.70	0.50	6422.2	3921.4	0.038	0.24	0.80
0.50	0.1	0.69	0.49	7888.2	4948.6	0.37	0.22	0.77
0.50	0.5	0.55	0.42	13413.9	9940.1	1.49	0.09	0.59
0.50	1	0.46	0.37	15445.6	12484.0	2.55	0.05	0.49
0.50	3	0.40	0.33	16132.2	13756.1	8.84	0.026	0.42
0.80	0.01	1.63	0.80	22347.3	1379.9	0.13	7.00	3.90
0.80	0.1	1.55	0.79	14244.3	1435.7	1.19	5.79	2.99
0.80	0.5	1.28	0.72	81241.1	17853.6	4.29	2.70	1.89
0.80	1	1.08	0.66	98335.0	33054.1	6.58	1.35	1.40
0.80	3	0.93	0.60	99797.8	43727.1	16.11	0.75	1.13

Please cite this article in press as: Farajzadeh R et al. The effect of heterogeneity on the character of density-driven natural convection of CO_2 overlying a brine layer. Adv Water Resour (2011), doi:10.1016/j.advwatres.2010.12.012

[39]. Indeed, the preservation of the statistical properties depends only on having a sufficiently large number of points to get a reasonably distributed set of phase angles ϕ_{kl} at enough locations to accurately and completely sample the spectral density. As shown in Ref. [30], fast Fourier transform algorithms do not always [40] give fields with the correct statistical properties.

The function $f(x_1,x_2)$ generated in Eq. (19) is normally distributed due to the central limit theorem and in its standard normal form. In many cases of practical interest the logarithm of the permeability is normally distributed [22]. In this case the logarithm of the permeability can be expressed by $\ln k = \mu + sf(x_1, x_2)$, where μ is the geometric average of the permeability k and $s = -\ln(1 - V_{DP})$ is the standard deviation of $\ln k$. The Dykstra–Parson coefficient V_{DP} is a measure of heterogeneity and assumes values in the range (0.6,0.8) and exceptionally up to (0.9) in cases of practical interest. It is therefore that the correlation structure of $\ln(k)$ is given by $\gamma_{\ln k}(h) = s^2(1 - \exp(-h/\lambda))$ if this structure is indeed exponential. It can be shown [41] that the variogram of k reads

$$\gamma_k(h) = \sigma^2 \frac{1 - e^{\gamma_{\ln k}(h)}}{1 - e^{-s^2}}, \tag{15}$$

where $\sigma^2 = \exp(2\mu + s^2)(\exp(s^2) - 1)$ is the variance of k. The average value of $k = \exp(\mu + 1/2s^2)$.

We have used Eq. (19) to generate 81×81 fields for $k = \exp(\mu + sf(x_1,x_2))$ using $N \times N = 201 \times 201$ frequency points. For each case with different values of V_{DP} and average permeability we generated 10 realizations of the fields by using different sequences of the random phase angles (ϕ_{kl}). As a rule of thumb we would need $(10C_V)^2$ realizations [22], where $C_V = \sqrt{(\exp(s^2) - 1)}$ is the coefficient of variation (average/standard deviation) to obtain statistically meaningful results, but this is technically impossible, because it requires per case hundreds of simulations, which each take few hours. However, by taking ten realizations per case we will obtain some idea of the variations that can be expected for these highly heterogeneous permeability fields.

4. Results and discussion

4.1. Homogeneous case

Fig. 2 shows the concentration profile of CO_2 for $Ra = 5000$ at different dimensionless times. The general features of the density-driven natural convection flow in a homogeneous porous medium are as follows (for details see Ref. [8]):

- Initially, the behavior of the system is controlled by diffusion. The time at which convection starts to dominate the flow, τ_c, decreases with increasing Rayleigh number. It has been shown that $\tau_c \propto 1/Ra^2$ [42,43].
- At early times, e.g. Fig. 2a and b, the number of fingers remain equal to the number put in the initial perturbation, i.e., 11.
- Some fingers grow faster than the others (Fig. 2c). As time elapses number of fingers decreases (Fig. 2d to g). The neighboring fingers coalesce by mutual interaction, and only few fingers survive to reach the bottom of the medium (Fig. 2g).
- The concentration contours suggest that the late-stage behavior of the mass transfer process cannot be precisely predicted by the early-stage behavior of the system. There will be some tenacity of the initial behavior and the pattern observed in the figures persists for some time before the number of fingers starts to decrease and starts to reflect intrinsic properties (see Fig. 15 in Ref. [8]).
- The stream-function profile preserves a similar pattern as the concentration profile (Fig. 3). This shows the importance of natural convection for the spreading of CO_2 in the cell. Moreover, it

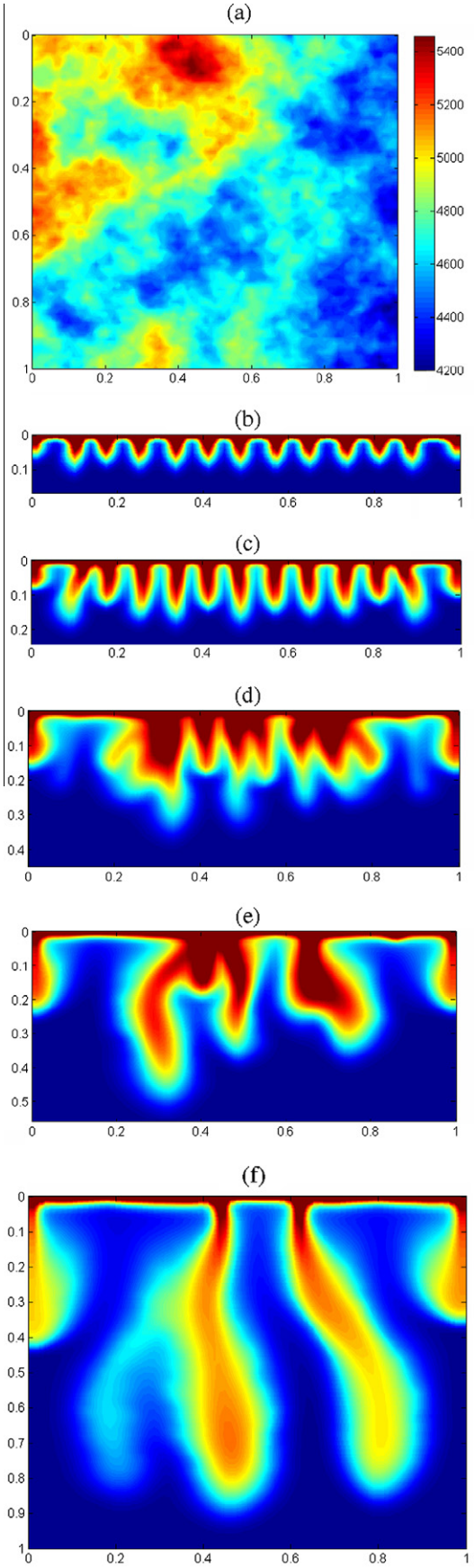

Fig. 4. Rayleigh field and concentration profiles of $V_{DP} = 0.1$ and $\lambda_R = 3$ (Case P13) at τ = (b) 0.0001, (c) 0.0003, (d) 0.00075, (e) 0.001, and (f) 0.002.

Please cite this article in press as: Farajzadeh R et al. The effect of heterogeneity on the character of density-driven natural convection of CO_2 overlying a brine layer. Adv Water Resour (2011), doi:10.1016/j.advwatres.2010.12.012

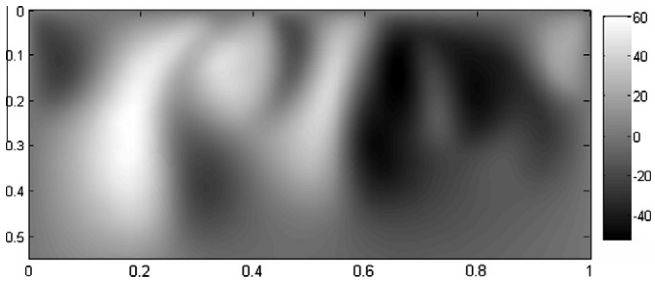

Fig. 5. Stream-function profile for Case P13 at $\tau = 0.001$ corresponding to concentration profile in Fig. 4e.

means that the dynamics of the non-linear behavior, i.e. fingering of CO_2 in the porous medium is governed by the flow field.

- The value of stream function decreases after reaching a maximum. This is in agreement with experimental observations indicating that convection effects diminish with time due to the increasingly more homogeneous concentration distribution as time progresses. The maximum Sherwood number or maximum value of the stream function is when CO_2 hits the bottom of the cell for the first time [4,44].
- The concentration front moves faster for the larger Rayleigh numbers implying that natural convection affects the mass transfer significantly for larger Rayleigh numbers (or aquifers with higher permeability).

4.2. Effect of heterogeneity

We follow the terminology proposed by Waggoner et al. [13] to interpret density-driven natural convection in a heterogeneous

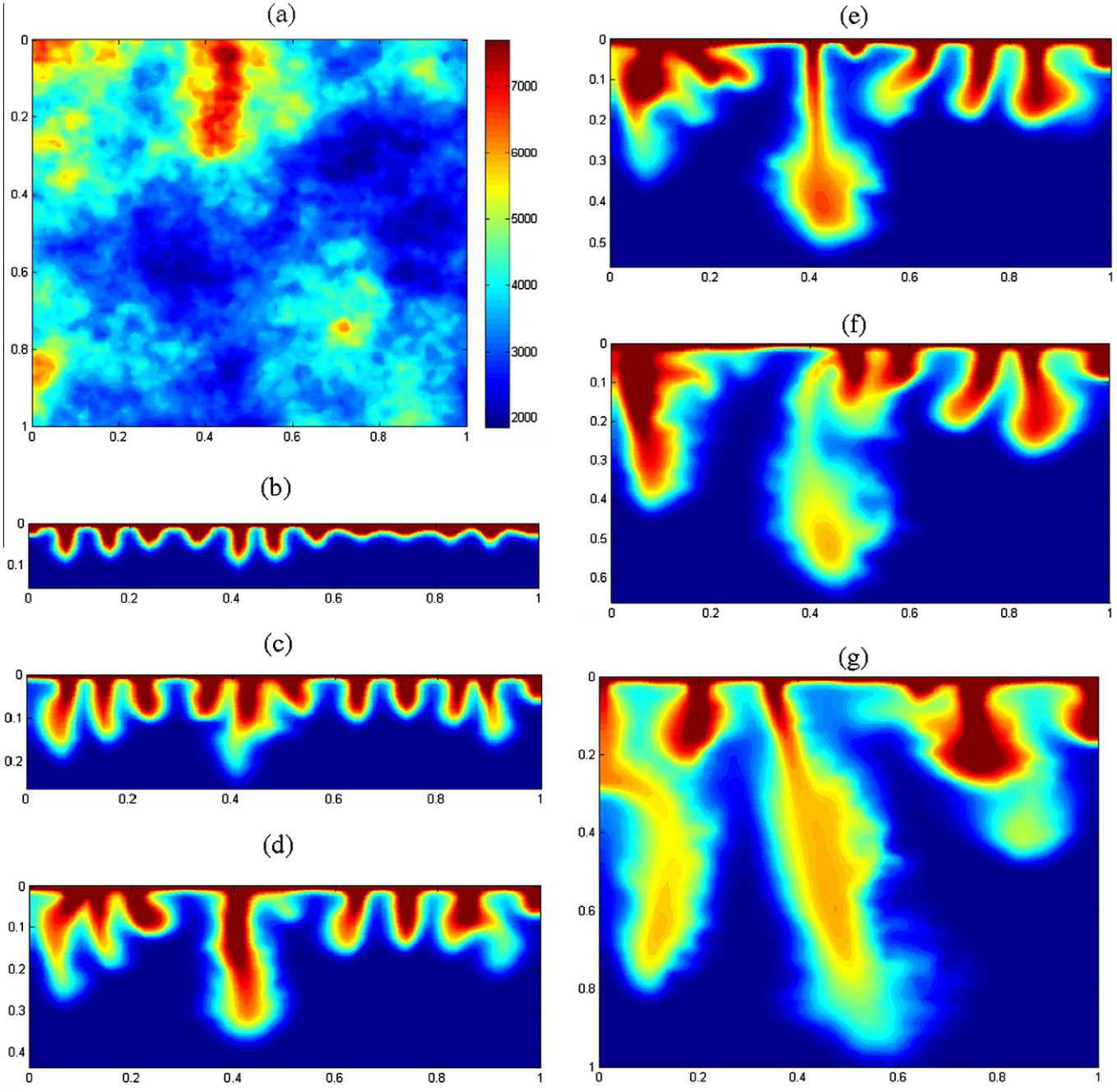

Fig. 6. Rayleigh (permeability) field and concentration profiles of $V_{DP} = 0.5$ and $\lambda_R = 3$ (Case P53) at $\tau =$ (b) 0.0001, (c) 0.0003, (d) 0.0005, (e) 0.00075, (f) 0.001 and (g) 0.002.

Please cite this article in press as: Farajzadeh R et al. The effect of heterogeneity on the character of density-driven natural convection of CO_2 overlying a brine layer. Adv Water Resour (2011), doi:10.1016/j.advwatres.2010.12.012

medium characterized by an average Dykstra–Parsons coefficient and a correlation length. We did not consider viscosity variations in our simulations. CO_2 dissolution increases the brine viscosity [45] and therefore the flow will resemble favorable miscible displacement ($M < 1$, M is the mobility ratio of the fluids) (Note that this reverse viscosity effect has impact on the initiation and growth of fingers especially when the effect of interface velocity [46] is considered [6]). This means that for our situations we use $M = 1$. According to Ref. [13] fingers disappear when $M = 1$; however, our situation concerns gravity-induced fingering and fingering disappears when $M + G < 1$, where G is the gravity number and defined as the ratio between the gravity and viscous forces [47].

We chose an average permeability that leads with other conditions to $Ra = 5000$. We generated 20 permeability fields represented by four levels of V_{DP} and λ_R. The V_{DP} values were 0.1, 0.3, 0.5, and 0.8. λ_R values were chosen to represent porous media from small to extremely large correlation; λ_R values were 0.001, 0.1, 0.5, 1, and 3. In all cases we chose $k_h = k_v$ and $L/H = 1$. To facilitate the discussion we have given a label to each case, as presented in Table 1 (P stands for point, the first number is V_{DP} and the second number is λ_R, e.g., Case P8P01 means the case with $V_{DP} = 0.8$ and $\lambda_R = 0.01$).

Table 2 summarizes examples of the output of our model for different realizations with $V_{DP} = 0.8$ and $\lambda_R = 1$. We notice that due to random nature of the stochastic model the output values are different for different realizations with the same input.

Table 3 provides the output of the program for $V_{DP} = 0.5$ and $V_{DP} = 0.8$ with different values for correlation length, λ_R. A variety of sample values related to the variance are calculated from output Rayleigh field of the two cases. We arbitrarily chose the seventh realization for this calculation. We observe that with increasing λ_R: (1) the estimated values of the heterogeneity index, the arithmetic and harmonic average increase, (2) the estimated values of V_{DP}, Koval factor and coefficient of variation decrease, and (3) the values of V_{DP} deviate further from the input value. Moreover, the sample variance is below the expected variance, especially for large correlation length. If the correlation length becomes infinity the variance would be zero. The reduction of coefficient of variation implies that we need a smaller number of realizations to conclude about the character of flow.

4.2.1. Fingering regime

At low V_{DP} independent of the correlation length we observe fingering behavior. By fingering we mean that the concentration plumes develop independently of the permeability structure. This aspect is illustrated in Fig. 4. Fig. 4a shows the Rayleigh (or permeability) field of one of the realizations of Case P13. Although the variance of the field is small ($\sigma^2_{\ln(Ra)} = 0.0023$), we observe that at the north and northwest of the field some clusters of gridcells have about 10% higher permeability than the average value, whilst the gridcells in the east part have about 10% lower permeability. The plumes develop equally well in the west and the east parts of the field. Fig. 4b to f depict the development of the plumes with time. The flow regime is similar to the homogeneous case explained in the previous section (Fig. 2). Fig. 5 shows the grey-level plot of the stream-function profile. The stream-function profile shows similar features as the concentration profile, i.e., the fingers are driven by the velocity profiles. The value of the stream function in this case is similar to the value in the homogenous case.

In Fig. 11 we show the variance of the concentration profiles as function of dimensionless time (Eqs. (15) and (16)). For comparison, we present all results (with the exception of $V_{DP} = 0.1$) on this figure. In each plot we show results of multiple realizations of each case. For $V_{DP} = 0.1$ (not shown in the figure) and Case P33 (top left plot) the variance increases faster than linear for all realizations implying that the flow is not diffusive. In Fig. 12 we present the cumulative mass dissolved as a function of time. The colored lines represent different realizations while the dashed line represents the dissolved mass of the homogeneous case on each plot. On a log–log scale the slope is between 0.5 and 1 meaning that the mass transfer is faster than diffusion alone, and therefore indicating the mixed diffusive–convective behavior in both homogeneous and heterogeneous media. When the correlation length is small the amount of dissolved CO_2 is larger than the homogeneous case for all of the realizations. When the correlation length becomes larger the mass of dissolved CO_2 in some realizations becomes lower than the homogenous case; however, the majority of the realizations show higher mass transfer rates. Moreover, the transfer rates of different realizations deviate further from the mean value when the correlation length becomes larger (the distance between lines becomes larger).

4.2.2. Channeling regime

Channeling regime occurs for medium V_{DP} values (moderate heterogeneity) independent of the correlation length. Note that when the correlation length becomes large the estimated V_{DP} of the medium becomes smaller (Table 2 and [30]). With channeling we mean that the plume develops along the high permeability streaks, i.e., the progress of CO_2 plumes are dominated by the permeability distribution pattern. An example of channeling is shown in Fig. 6. Fig. 6a shows the Rayleigh field of one of the realizations of Case P53. We observe high permeability streaks at the north and northwest parts of the field. Fig. 6b to f show indeed that faster plume development occurs along the high permeability regions. Due to channeling water is bypassed and thus dissolution is not efficient. Because of the higher variance of the permeability field

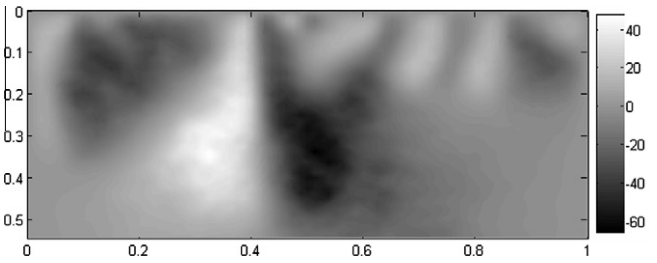

Fig. 7. Stream-function profile for Case P53 at $\tau = 0.00075$ corresponding to concentration profile in Fig. 6e.

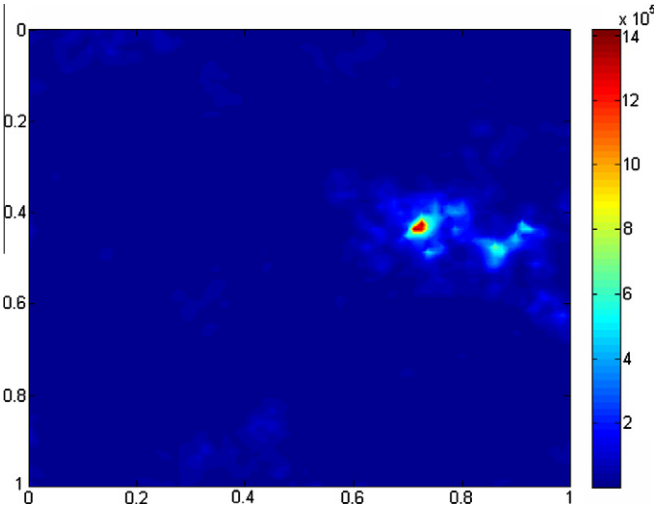

Fig. 8. Rayleigh field of $V_{DP} = 0.8$ and $\lambda_R = 0.1$ (Case P8P1).

Please cite this article in press as: Farajzadeh R et al. The effect of heterogeneity on the character of density-driven natural convection of CO_2 overlying a brine layer. Adv Water Resour (2011), doi:10.1016/j.advwatres.2010.12.012

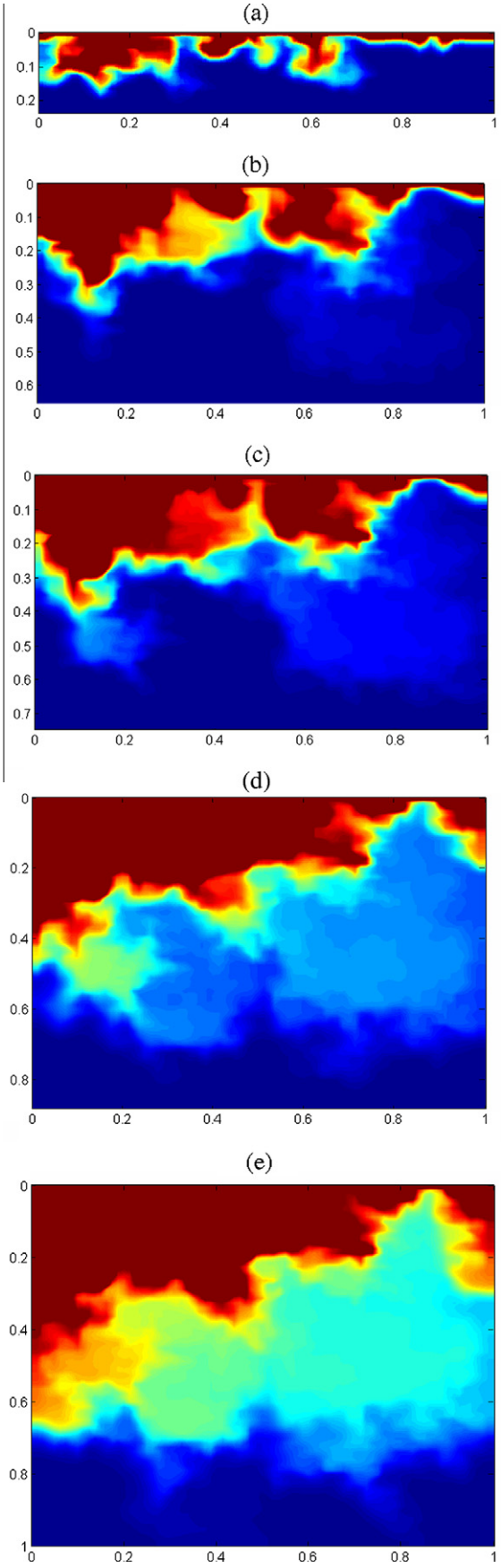

Fig. 9. Concentration profiles of $V_{DP} = 0.8$ and: $\lambda_R = 0.1$ (Case P8P1) at τ = (a) 0.0001, (b) 0.0005, (c) 0.00075, (d) 0.0015, and (e) 0.0025.

compared to the previous case ($\sigma^2_{\ln(Ra)} = 0.01 > 0$), some of realizations show lower dissolution rate than the homogenous case; however, in average the dissolution rate for heterogeneous media is higher than for the homogeneous case. Similar to the fingering regime, the growth of variance of concentration profile in corresponding plots in Fig. 11 is faster than linear and slower than square root of time, implying mixed convective–dispersive flow. Fig. 7 shows the stream-function profile of this example. It illustrates that the fluid velocity is higher in high permeability region and lower in low permeability regions. The magnitude of the stream function is comparable to the fingering example.

4.2.3. Dispersive regime

For large heterogeneities when the correlation length is small, the concentration profile progresses proportional to the square root of the time. This regime is dispersive as bypassing of water in channels is not observed in the simulations and therefore the mixing is more efficient. Fig. 8 shows the Rayleigh field of one of the cases in which we observe the dispersive behavior. The Rayleigh field has a very large variance ($\sigma^2_{\ln(Ra)} = 2.25$) and contains grid cells with permeability values that are smaller than 100 and values larger than 10^6. The concentration profile of this Rayleigh field is presented in Fig. 9a through e. The mixing zone develops as a result of the physical dispersion plus the mixing caused by the heterogeneities of small λ_R. The time at which CO_2 reaches the bottom is larger than the fingering and channeling regimes and consequently the transfer rate of CO_2 is higher in the dispersive regime. As shown in Fig. 11 the mixing zone in all realizations progresses proportional to the square root of the time (if the variance is proportional to time, the mixing zone progresses proportional to the square root of time). This implies that for fields with large variance and small correlation length, the mass transfer of CO_2 into water can be described with a dispersion model with large effective dispersion coefficient to account for the velocity induced by density-driven natural convection. Fig. 10 shows the stream function profile of this case. As expected the stream function has very large values in high permeability grid cells (note the similarities between Figs. 8 and 10).

Fig. 13 shows the schematic diagram of the flow regime introduced by Ref. [13]. This plot is generated based on Fig. 11, where we plot the variance of concentration profile as a function of time. For Case P83, from the simulations we observe that for all realizations the CO_2 plumes progress along the high permeable regions; however, as Fig. 11 (top right plot) shows the plot of variance of concentration profile vs. time is linear implying the flow can be dispersive. Therefore, in Fig. 13 for large heterogeneities the boundary between dispersive and channeling regimes has been shown by a dashed curve.

Comparison of the flow-regime map shown in Fig. 13 with that in Fig. 3 of Ref. [13] reveals some similarities and differences

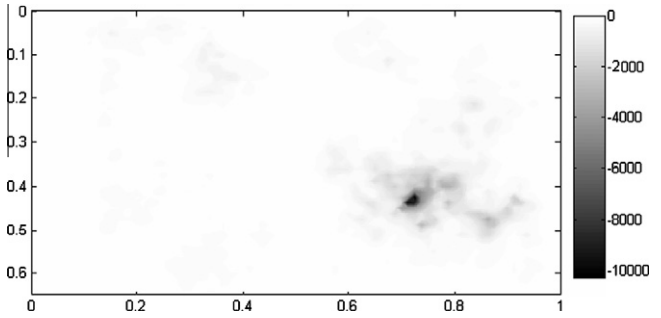

Fig. 10. Stream-function profile for Case P8P1 at $\tau = 0.00075$ corresponding to concentration profile in Fig. 8e.

Please cite this article in press as: Farajzadeh R et al. The effect of heterogeneity on the character of density-driven natural convection of CO_2 overlying a brine layer. Adv Water Resour (2011), doi:10.1016/j.advwatres.2010.12.012

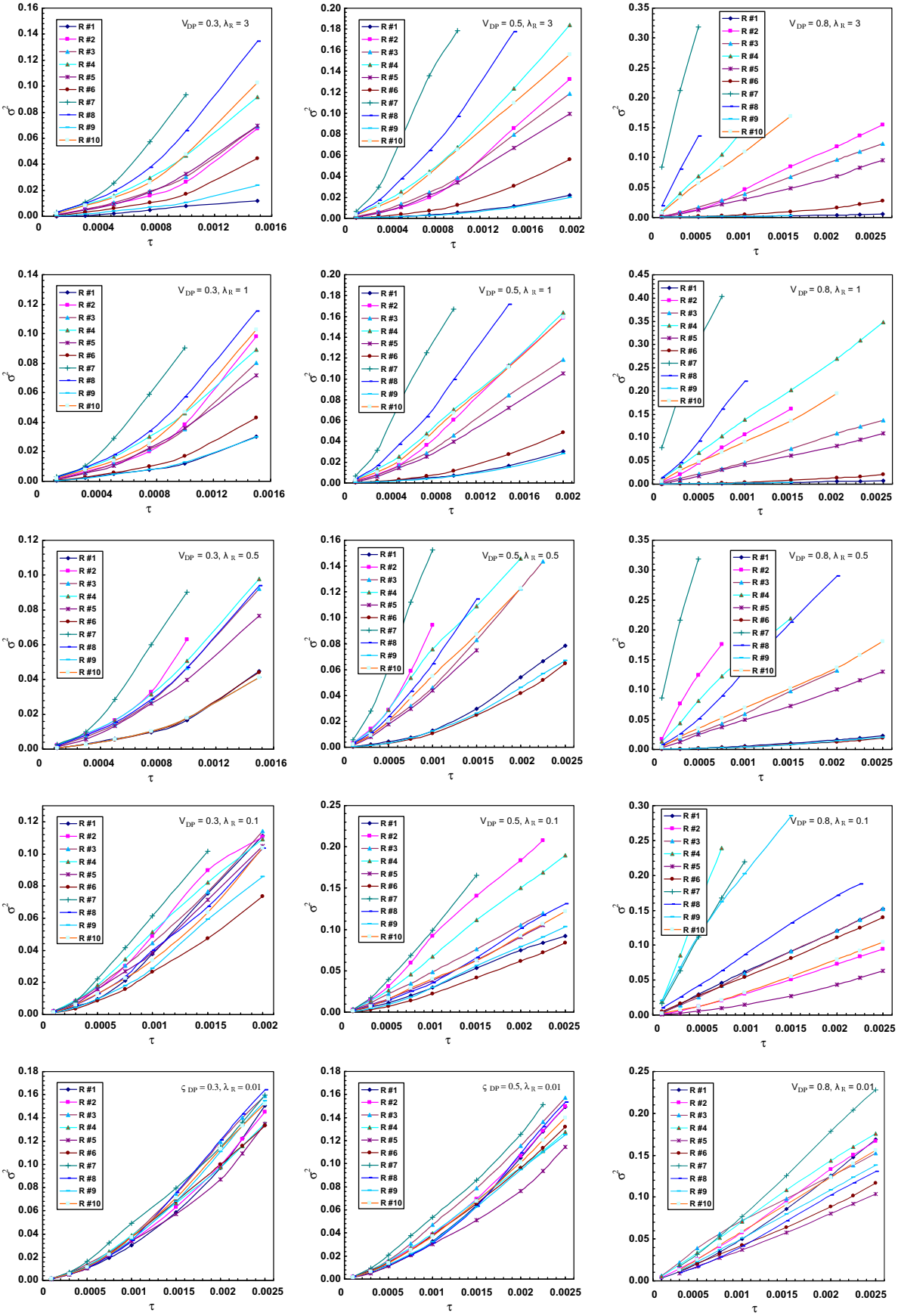

Fig. 11. Variance of the average concentration in the medium a function of dimensionless time for multiple realizations of different simulations.

Please cite this article in press as: Farajzadeh R et al. The effect of heterogeneity on the character of density-driven natural convection of CO_2 overlying a brine layer. Adv Water Resour (2011), doi:10.1016/j.advwatres.2010.12.012

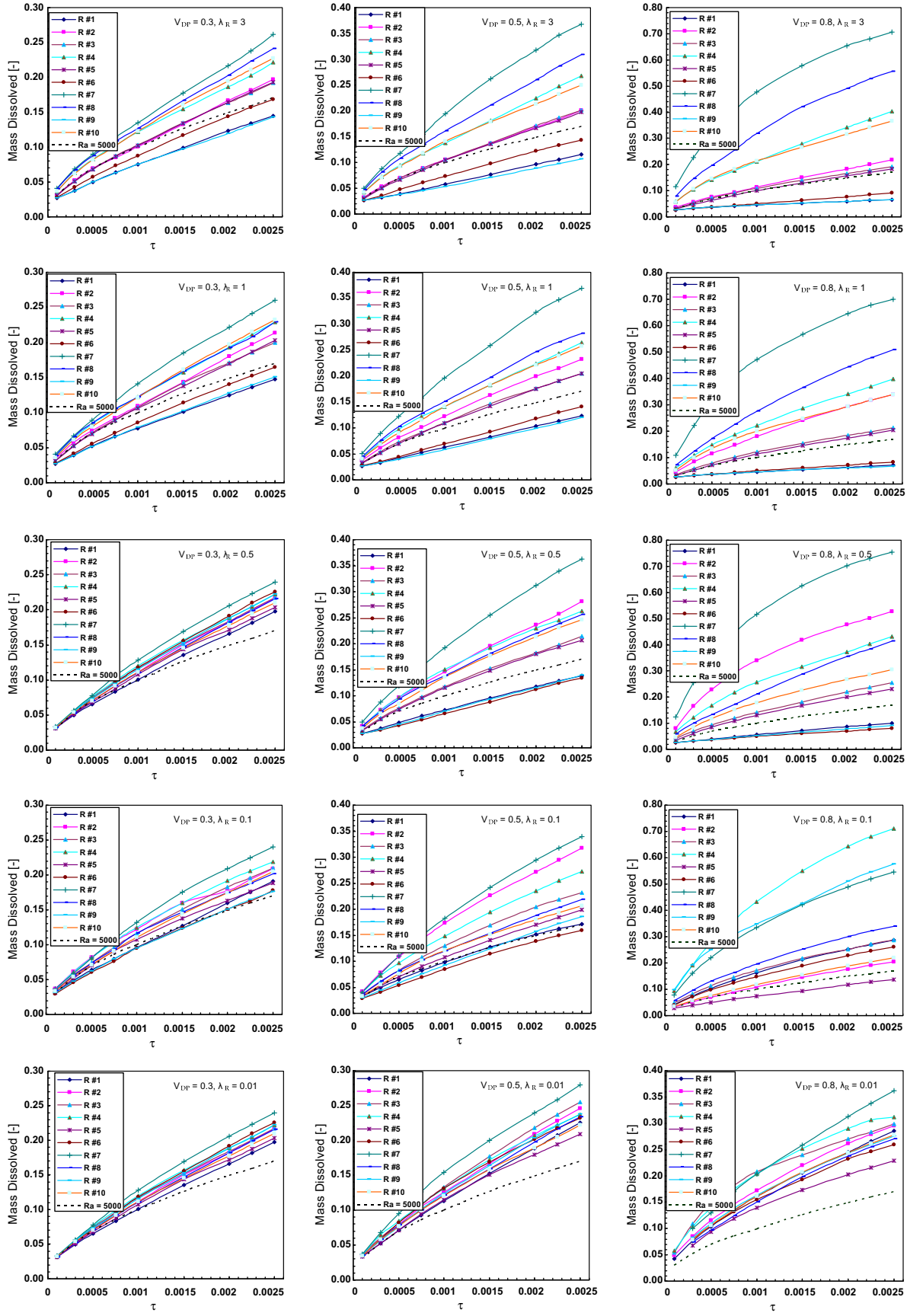

Fig. 12. Dimensionless mass of dissolved CO_2 as a function of dimensionless time for multiple realizations of different simulations.

Please cite this article in press as: Farajzadeh R et al. The effect of heterogeneity on the character of density-driven natural convection of CO_2 overlying a brine layer. Adv Water Resour (2011), doi:10.1016/j.advwatres.2010.12.012

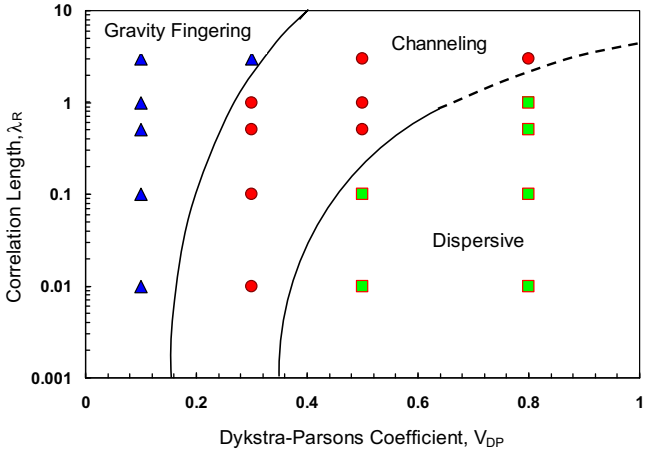

Fig. 13. Flow regime map for density-driven natural convection (Ra = 5000).

between the gravity and viscous instabilities. In both cases three flow regimes (fingering, channeling, and dispersive) are discerned. Fingering seems to be characteristic of homogeneous media and the fluid flow behavior is dominated by the heterogeneity for both gravity and viscous instabilities. Moreover, in both cases characterization of the flow only with the permeability variance is not entirely correct and it seems that the correlation length of the medium is as important as the heterogeneity. Despite these similarities, the position of the channeling and dispersive regimes are altered in the two figures. In the gravitationally unstable flow, at low heterogeneities we observe channeling and as the heterogeneity increases (when correlation length is smaller than 2) the transition from channeling to dispersive flow occurs. However, in Fig. 3 of Ref. [13] at large heterogeneities, the flow is dispersive when the correlation length of the system is very small. The concept of a critical correlation length (λ_R above which, at a given V_{DP}, the transition from dispersive to channeling happens) is applicable for both cases.

4.2.4. Implications of the results

Aquifers (or reservoirs) are in general heterogeneous with V_{DP} values typically between 0.6 and 0.8 (and even higher). Our results show that gravity-induced fingering does not occur in realistic porous media, i.e., when the heterogeneity is not small. This was also observed for viscous fingering by Refs. [13,14,48] for miscible displacement and by Ref. [15] for immiscible displacement. At moderate heterogeneity channels form along the high permeability streaks and the development of CO_2 plumes strongly correlates with the permeability distribution of the field. The effect of large heterogeneity depends on the arrangement of the permeability field. Up to $1 < \lambda_R < 3$ there is no bypassing and the dissolution of CO_2 in water can be characterized by a dispersion model, which employs an effective dispersion coefficient to account for dissolution or transfer rate of CO_2 into water. When the correlation length is large the estimated V_{DP} of the field becomes lower and therefore channeling regime occurs. At very large λ_R values the medium becomes layered and thus channels will form. This is summarized in Fig. 13.

For our simulation conditions, efficient storage of CO_2 occurs in the heterogeneous reservoirs with small correlation length, although for all heterogeneous cases of practical relevance the transfer rates are higher than for the homogenous case. This suggests that simulations in the homogenous porous media are not realistic and underestimate the transfer rates. When studying the effect of heterogeneity on density-driven natural convection flow of CO_2 a single realization does not give a representative estimate of the transfer rate; therefore, more realizations are required to estimate the variance of the transfer rates between the realizations. Moreover, we find no correlation between the mass of dissolved CO_2 with the heterogeneity measures.

5. Conclusions

- Following the work of Waggoner et al. [13] we studied the effect of heterogeneity on the character of natural convection flow when CO_2 overlays a brine column.
- Heterogeneity of the permeability (or Rayleigh) fields was characterized through a Dykstra–Parsons coefficient, V_{DP}, and their spatial arrangement was represented by a dimensionless correlation length, λ_R. We generated 10 realizations for each permeability field.
- Our numerical simulations demonstrate three flow regimes (fingering, dispersive, and channeling) for density-driven natural convection flow in heterogeneous media.
- At low heterogeneity characterized by small V_{DP}'s gravity-induced fingering is dominant pattern. Fingering will not occur in realistic porous media.
- At moderate heterogeneity (medium V_{DP}'s or large V_{DP}'s with large λ_R) the flow is dominated by the permeability field structure, i.e., channels form and CO_2 plumes progress along the high permeability streaks.
- At large heterogeneity when the correlation length of the field is small the flow is dispersive. In this regime the concentration travels proportional to square root of time and therefore it can be represented by a dispersion model.
- Numerical simulations in homogenous porous media underestimate the mass transfer rate of CO_2 into water. The rate of CO_2 dissolution in heterogeneous media is larger than in homogeneous media. This means that larger volumes of CO_2 can be stored in heterogeneous media.
- We found no correlation between the mass of dissolved CO_2 in water and the heterogeneity measures.

References

[1] Gmelin L, Gmelin Handbuch der anorganischen Chemie, 8. Auflage. Kohlenstoff, Teil C3, Verbindungen; 1973. p. 64–75.
[2] Yang Ch, Gu Y. Accelerated mass transfer of CO_2 in reservoir brine due to density-driven natural convection at high pressures and elevated temperatures. Ind Eng Chem Res 2006;45:2430–6.
[3] Farajzadeh R, Barati A, Delil HA, Bruining J, Zitha PLJ. Mass transfer of CO_2 into water and surfactant solutions. Petrol Sci Technol 2007;25:1493.
[4] Farajzadeh R, Bruining J, Zitha PLJ. Enhanced mass transfer of CO_2 into water: experiment and modeling. Ind Eng Chem Res 2009;48(9):4542–52.
[5] Riaz A, Hesse M, Tchelepi A, Orr FM. Onset of convection in a gravitationally unstable diffusive boundary layer in porous medium. J Fluid Mech 2006;548:87–111.
[6] Meulenbroek B, Farajzadeh R, Bruining J. Multiple scale analysis of the stability of a diffusive interface between aqueous and gaseous CO_2. J Fluid Mech submitted for publication.
[7] Hassanzadeh H, Pooladi-Darvish M, Keith D. Scaling behavior of convective mixing, with application to CO2 geological storage. AIChE J 2007;53(5):1121–31.
[8] Farajzadeh R, Salimi H, Zitha PLJ, Bruining J. Numerical simulation of density-driven natural convection with application for CO_2 injection projects. Int J Heat Mass Transf 2007;50:5054.
[9] Green C, Ennis-Kinga J, Pruessc K. Effect of vertical heterogeneity on long-term migration of CO2 in saline formation. Energy Proc 2009;1(1):1823–30.
[10] Nield DA, Simmons CT. A discussion on the effect of heterogeneity on the onset of convection in a porous medium. Transp Porous Media 2007;68:413–21.
[11] Ranganathan P, Bruining J, Zitha PLJ. Numerical simulation of natural convection in heterogeneous porous media for CO_2 geological storage. Transp Porous Media, in press.
[12] Farajzadeh R, Farshbaf Zinati F, Zitha PLJ, Bruining J. Density driven natural convection in layered and anisotropic porous media. In: Proceedings of the 11th European conference on mathematics in oil recovery (ECMOR X1), Bergen, Norway, 8–11 September 2008.

Please cite this article in press as: Farajzadeh R et al. The effect of heterogeneity on the character of density-driven natural convection of CO_2 overlying a brine layer. Adv Water Resour (2011), doi:10.1016/j.advwatres.2010.12.012

[13] Waggoner JR, Castillo JL, Lake LW. Simulation of EOR processes in stochastically generated permeable media. SPE Form Eval 1992;7(2):173–80.
[14] Sorbie KS, Farag Feghi, Pickup KS, Ringrose PS, Jensen JL. Flow regimes in miscible displacements in heterogeneous correlated random fields. SPE Adv Technol Ser 1994;2(2):78–87.
[15] Chang YB, Pope GA, Sepehrnoori K. CO_2 flow patterns under multiphase flow: heterogeneous field-scale conditions. SPE Reservoir Eng 1993;9(3):208–16.
[16] Guçeri S, Farouk B. Numerical solutions in laminar and turbulent natural convection. In: Kakac S, Aung W, Viskanta R, editors. Natural convection, fundamentals and applications. Hemisphere Publication; 1985. p. 615–55.
[17] Landau LD, Lifshitz EM. Statistical physics: course of theoretical physics, second revised English ed., vol. 5. Pergamon Press; 1969.
[18] Gunn RD, Krantz WB. Reverse combustion instabilities in tar sands and coal. SPE 1980;6735-PA.
[19] Yortsos YC, Xu B, Salin D. Phase diagram of fully developed drainage in porous media. Phys Rev Lett 1997;79(23).
[20] Parlar M, Yortsos YC. Percolation theory of steam/water relative permeability. SPE 1987;16969.
[21] Gelhar LW. Stochastic subsurface hydrology. Prentice Hall Professional Technical Reference; 1993.
[22] Jensen JL, Lake LW, Corbett P, Goggin D. Statistics for petroleum engineers and geoscientists. Handbook of petroleum exploration and production 2 (HPEP). Elsevier; 2000.
[23] Koval EJ. A method for predicting the performance of unstable miscible displacement in heterogeneous media. SPE J 1963;3(2):145–54.
[24] Gelhar LW, Axness CL. Three-dimensional stochastic analysis of macrodispersion in aquifers. Water Resour Res 1983;19(1):161–80.
[25] Lasseter TJ, Waggoner JR, Lake LW. Reservoir heterogeneity and its influence on ultimate recovery. In: Lake LW, Carroll HB, editors. Reservoir characterization. Orlando, Florida: Academic Press; 1986. 659 p.
[26] King MJ, Blunt MJ, Manseld M, Christie MA. Rapid evaluation of the impact of heterogeneity on miscible gas injection. In: Proceedings of the 7th European Symposium on IOR, (Moscow, Russia), vol. 2; 1993. p. 398–407.
[27] Journel AG, Huijbregts CJ. Mining geostatistics. London: Academic Press; 1978. 600 p..
[28] Deutsch CV, Journel AG. GSLIB; geostatistical software library and user's guide. New York: Oxford University Press; 1992. 340 p.
[29] Bruining J. Modeling reservoir heterogeneity with fractals: Enhanced Oil and Gas, Recovery Research Program, Rep. No. 92-5, Center for Petroleum and Geosystems Engineering, University of Texas, Austin; 1992. 88 p.
[30] Bruining J, van Batenburg DW, Lake LW, Yang AP. Flexible spectral methods for the generation of random fields with power-law semivariograms. Math Geol 1997;29:823–48. ISSN: 0882-8182.
[31] Jensen JL, Lake LW. The influence of sample size and permeability distribution on heterogeneity measures. SPE Reservoir Eng 1988;3(2):629–37.
[32] Rice SO. Mathematical analysis of random noise. In: Wax N, editor. Selected papers on noise and stochastic processes. NewYork: Dover Publ. p. 133–294.
[33] Shinozuka M, Jan CM. Digital simulation of random processes and its applications. J Sound Vibration 1972;25(1):357–68.
[34] Borges MR, Pereira F, Amaral Souto HP. Efficient generation of multi-scale random fields: a hierarchical approach. Commun Numer Methods Eng 2009. doi:10.1002/cnm.1134.
[35] Ebrahimi F, Sahimi M. Grid coarsening, simulation of transport processes in, and scale-up of heterogeneous media: application of multiresolution wavelet transformations. Mech Mater 2006;38:772–85.
[36] Elfeki AMM, Dekking FM, Kraaikamp C, Bruining J. Influence of fine-scale heterogeneity patterns on large-scale behaviour of miscible transport in porous media. Petr Geosci 2002;8(2):159–65.
[37] Dekking FM, Kraaikamp C, Elfeki AM, Bruining J. Multiscale and multiresolution stochastic modelling of subsurface heterogeneity by tree-indexed Markov chains. Comput Geosci 2001;5(1):47–60.
[38] Bárdossy A. Copula-based geostatistical models for groundwater quality parameters. Water Resour Res 2006;42(11):W11416.
[39] Press WH, Teukolsky SA, Vetterling WT, Flannery BP. Numerical Recipes in C. The art of scientific computing. Cambridge University Press; 1992.
[40] Monnig Nathan D, Benson David A, Meerschaert Mark M. Ensemble solute transport in two-dimensional operator-scaling random fields. Water Resour Res 2008;44:W02434. doi:10.1029/2007WR005998.
[41] Vanmarcke E. Random field analysis and synthesis. Cambridge, Massachusetts: M.I.T.Press; 1983. 382 p.
[42] Xu X, Chen Sh, Zhang D. Convective stability analysis of the long-term storage of carbon dioxide in deep saline aquifers. Adv Water Res 2006;29: 397–407.
[43] Ennis-King J, Paterson L. Role of convective mixing in the long-term storage of carbon dioxide in deep saline aquifers. SPE J 2005;10(3):349.
[44] Farajzadeh R, Delil HA, Zitha PLJ, Bruining J. Enhanced mass transfer of CO_2 into water and oil by natural convection In: SPE 107380. EUROPEC London, The UK; 2007.
[45] Bando S, Takemura F, Nishio M, Hihara E, Akai M. Viscosity of aqueous NaCl solutions with dissolved CO_2 at (30 to 60) C and (10 to 20) MPa. J Chem Eng Data 2004;49:1328–32.
[46] Haugen KB, Firoozabadi A. Composition a the interface between multi-component nonequilibrium fluid phases. J Chem Phys 2009;130:064707.
[47] Dake LP. Fundamentals of reservoir engineering. Developments in petroleum science, vol. 8. Elsevier; 1978.
[48] Li D, Lake LW. Scaling fluid flow through heterogeneous permeable media. SPE Adv Technol 1995;3(1):188–97.
[49] Bear J. Dynamics of fluids in porous materials. American Elsevier; 1972.
[50] Gómez-Hernández JJ, Wen XH. To be or not to be multi-Gaussian? A reflection on stochastic hydrogeology. Adv Water Resour 1998;21(1):47–61.

Please cite this article in press as: Farajzadeh R et al. The effect of heterogeneity on the character of density-driven natural convection of CO_2 overlying a brine layer. Adv Water Resour (2011), doi:10.1016/j.advwatres.2010.12.012